nature microbiology

ARTICLES

PUBLISHED: 19 SEPTEMBER 2016 | ARTICLE NUMBER: 16172 | DOI: 10.1038/NMICROBIOL.2016.172

Bacterial cell wall biogenesis is mediated by SEDS and PBP polymerase families functioning semi-autonomously

Hongbaek Cho[1†], Carl N. Wivagg[2†], Mrinal Kapoor[2†], Zachary Barry[2], Patricia D. A. Rohs[1], Hyunsuk Suh[3], Jarrod A. Marto[3,4], Ethan C. Garner[2*] and Thomas G. Bernhardt[1*]

Multi-protein complexes organized by cytoskeletal proteins are essential for cell wall biogenesis in most bacteria. Current models of the wall assembly mechanism assume that class A penicillin-binding proteins (aPBPs), the targets of penicillin-like drugs, function as the primary cell wall polymerases within these machineries. Here, we use an *in vivo* cell wall polymerase assay in *Escherichia coli* combined with measurements of the localization dynamics of synthesis proteins to investigate this hypothesis. We find that aPBP activity is not necessary for glycan polymerization by the cell elongation machinery, as is commonly believed. Instead, our results indicate that cell wall synthesis is mediated by two distinct polymerase systems, shape, elongation, division, sporulation (SEDS)-family proteins working within the cytoskeletal machines and aPBP enzymes functioning outside these complexes. These findings thus necessitate a fundamental change in our conception of the cell wall assembly process in bacteria.

An essential cell wall surrounds most bacteria, protecting their cytoplasmic membrane from osmotic rupture[1]. This structure is built from the heteropolymer peptidoglycan (PG), which consists of glycan chains, with attached peptides used to form interstrand crosslinks that generate a matrix-like shell. PG biogenesis is disrupted by many of our most effective antibiotics and remains an attractive target for the development of new therapies to counter the growing problem of drug-resistant infections[2].

Rod-shaped bacteria typically use two essential cell wall biogenesis machines to grow and divide[1]. Cell elongation is promoted by the Rod system, which consists of several integral membrane proteins, including RodA, a shape, elongation, division, sporulation (SEDS)-family protein, and PBP2, a class B penicillin-binding protein (bPBP) with transpeptidase (TP) activity that forms cell wall crosslinks. The Rod system is organized by dynamic filaments of the actin homologue MreB, which are thought to direct new cell wall synthesis to establish and maintain rod shape[1,3–7] (Fig. 1a). Cell division is mediated by a different multi-protein machine, the divisome, which is organized by the tubulin homologue FtsZ (refs 1 and 8). The proteins composing the divisome are largely distinct from those of the Rod system, but it contains homologous factors for PG synthesis like the SEDS-family protein FtsW and PBP3, a bPBP related to PBP2 (ref. 1).

Due to the lack of specific *in vivo* assays, the enzymes that synthesize PG glycans within the MreB- and FtsZ-directed machines have not been clearly defined. The generally accepted model is that glycan polymerization by these systems is mediated by the class A PBPs (aPBPs), which are bifunctional enzymes possessing both PG glycosyltransferase (PGT/polymerase) and TP (crosslinking) activity[1]. In support of this idea, aPBP activity is indispensable for growth in many organisms[9–11]. Additionally, aPBP-like PGT domains have been the only enzymes known to possess PG polymerase activity[12]. However, this functional assignment fails to account for the observation that certain Gram-positive bacteria, including *Bacillus subtilis* and some species of *Enterococcus*, are viable and continue producing PG in the absence of identifiable aPBP-like domains[13,14]. Moreover, it has remained unclear whether the unidentified polymerase activity suggested by these findings is unique to certain Gram-positive species or broadly distributed in bacteria.

An *in vivo* assay for PG polymerase activity

To determine if PG synthesis by the Rod system is dependent on aPBP function, we developed an *in vivo* assay to monitor PG polymerase activity. The assay is based on the observation that TP inactivation by β-lactams in *E. coli* leads to the formation of uncrosslinked PG glycans that are rapidly degraded into turnover products, which can then be quantified as an indirect measure of PG polymerase activity[15,16] (Fig. 1b). Because it specifically targets PBP2, the β-lactam mecillinam facilitates the measurement of polymerase activity within the Rod system[15]. In this assay, cells are first blocked for divisome function, thus eliminating its contribution to synthesis and focusing the measurement on Rod system activity. Under these conditions, mecillinam treatment reduces the ability of cells to incorporate the radiolabelled PG precursor [^{3}H]-diaminopimelic acid ([^{3}H]-DAP) into the PG matrix. Instead, a dramatic increase in labelled turnover products is observed, which reflects PG polymerization by the Rod system[15] (Fig. 2a,b, samples 1 and 2). Consistent with this interpretation, simultaneous mecillinam treatment and inactivation of the Rod system with A22, an MreB polymerization antagonist, dramatically reduces both synthesis and turnover (Fig. 2a,b, samples 1 and 6)[15].

The *E. coli* Rod system does not require aPBP activity

The effect of aPBP inactivation on Rod system activity was investigated using an *E. coli* strain (HC533) producing a modified PBP1b as its only aPBP. This variant of PBP1b, referred to as ^{MS}PBP1b, harbours a Ser247Cys substitution in its PGT domain, allowing specific inhibition

[1]Department of Microbiology and Immunobiology, Harvard Medical School, Boston, Massachusetts 02115, USA. [2]Department of Molecular and Cellular Biology, Harvard University, Cambridge, Massachusetts 02138, USA. [3]Department of Biological Chemistry and Molecular Pharmacology, Harvard Medical School, Boston, Massachusetts 02115, USA. [4]Department of Cancer Biology and Blais Proteomics Center, Dana-Farber Cancer Institute, Boston, Massachusetts 02215, USA. †These authors contributed equally to this work. *e-mail: thomas_bernhardt@hms.harvard.edu; egarner@g.harvard.edu

© 2016 Macmillan Publishers Limited, part of Springer Nature. All rights reserved.

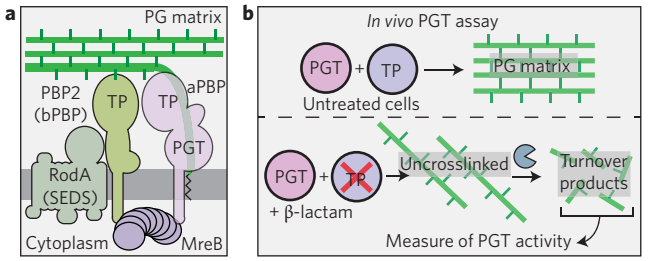

Figure 1 | The Rod system and an *in vivo* assay of peptidoglycan (PG) polymerase activity. a, Diagram of the currently accepted model for PG biogenesis by the Rod system. Polymers of the actin-like MreB protein organize a complex of membrane proteins including RodA, PBP2 and an aPBP. Glycan polymerization and crosslinking by this complex is thought to be promoted primarily by the peptidoglycan glycosyltransferase (PGT) and transpeptidase (TP) activities of aPBPs with additional TP activity provided by PBP2. **b**, In untreated cells, PG polymerization and crosslinking by PGT and TP enzymes, respectively, are tightly coupled to form the PG matrix (upper panel). When TP activity is inhibited by a β-lactam, the polymerase working with the blocked TP continues to produce uncrosslinked glycans that are rapidly degraded into fragments that can be isolated and quantified as a measure of polymerase activity (lower panel).

of its polymerase activity using the cysteine-reactive reagent MTSES (2-sulfonatoethyl methanethiosulfonate)[17]. In the absence of MTSES, HC533 cell growth and morphology were indistinguishable from wild-type (WT) cells, and PG biogenesis activity was similar to cells producing an unaltered copy of PBP1b (Supplementary Fig. 1a–c). Treatment of [^{3}H]-DAP-labelled, division-inhibited HC533 cells with MTSES reduced PG synthesis without stimulating turnover (Fig. 2a,b, sample 3). This level of PG synthesis inhibition was similar to that observed following treatment of an outer-membrane defective strain with the canonical PGT inhibitor moenomycin (Supplementary Fig. 1d). Surprisingly, however, these MTSES-treated cells retained significant (~20%) PG synthetic activity (Fig. 2a,b, sample 3). This synthesis was not due to residual ^{MS}PBP1b activity, as analysis by mass spectrometry indicated that the protein was fully modified by MTSES (Supplementary Table 1 and Supplementary Fig. 2), and experiments with the β-lactam cefsulodin (described in the penultimate section) show that this treatment completely disrupts aPBP-mediated PG polymerization. Thus, the observed MTSES-resistant synthesis suggests that, like Gram-positive bacteria, *E. coli* also encodes a non-aPBP-mediated PGT activity. This MTSES-resistant synthesis was inhibited by co-treatment with A22, and was fully converted to PG turnover products with mecillinam co-treatment (Fig. 2a,b, samples 4 and 7), indicating that the non-aPBP PGT enzyme resides in the Rod system.

Fluorescently tagged MreB displays a dynamic subcellular localization with many discrete foci rotating around the circumference of the cell cylinder[4–6]. As MreB rotation is halted by β-lactams and other PG synthesis inhibitors, this motion is thought to reflect new cell wall synthesis[4–6]. To monitor the effect of aPBP inactivation on MreB dynamics, we followed the motion of a functional mNeonGreen-MreB sandwich fusion (MreB-^{SW}mNeon) (Supplementary Fig. 3) in cells possessing ^{MS}PBP1b as the sole aPBP. MreB-^{SW}mNeon foci continued rotating following aPBP inhibition by MTSES at a speed undifferentiable from untreated cells (20 nm s^{-1}), until the lack of aPBP activity caused cell lysis (Fig. 2c,d and Supplementary Video 1). Thus, both radiolabelling and imaging indicate that aPBPs are not required for PG polymerization by the Rod system in Gram-negative bacteria, as is widely believed.

RodA and PBP2 display circumferential motion in *E. coli*

Results from a parallel *B. subtilis* study indicate that RodA functions as a PG polymerase[18]. We therefore hypothesized that RodA might also be responsible for the aPBP-independent PG synthesis we observed in *E. coli*. If true, we reasoned that *E. coli* RodA should

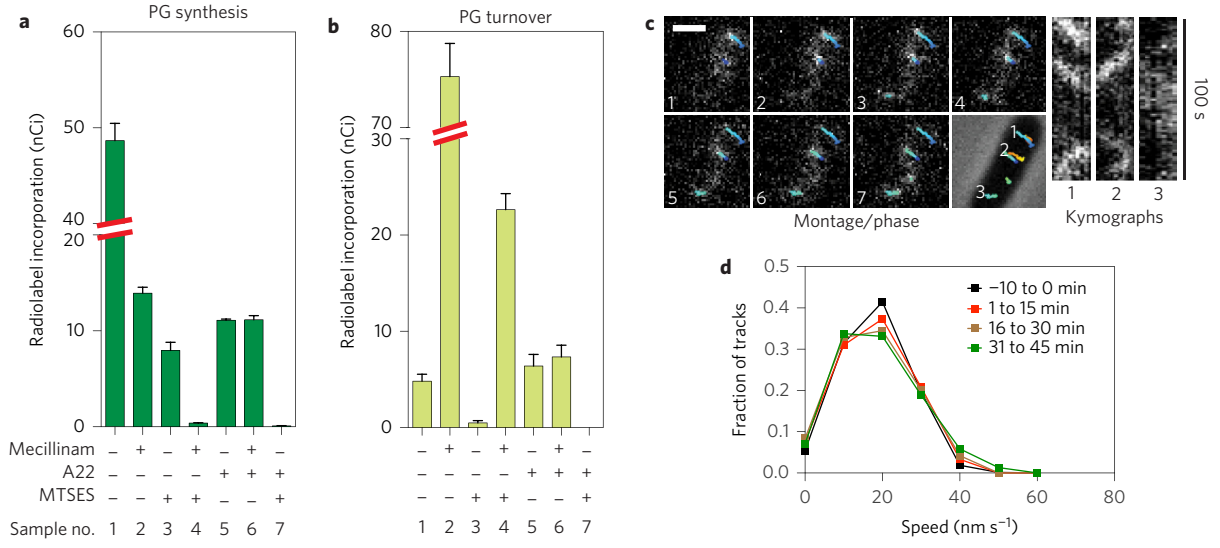

Figure 2 | PG polymerization by the Rod complex does not require aPBP activity. a,**b**, Cells of HC533(attλHC739) (Δ*lysA* Δ*ampD* Δ*ponA* Δ*pbpC* Δ*mtgA* ^{MS}*ponB* (P$_{tac}$::*sulA*)) producing SulA to block cell division were pulse labelled with [^{3}H]-mDAP following treatment with the indicated compound(s). Turnover products were extracted with hot water and quantified by HPLC and in-line radiodetection. PG incorporation was determined by digesting the pellets resulting from the hot water extraction with lysozyme and quantifying the amount of label released into the supernatant by scintillation counting. Compound concentrations used: mecillinam (10 μg ml^{-1}), A22 (10 μg ml^{-1}), MTSES (1 mM). Results are the average of three independent experiments. Error bars represent the standard error of the mean (s.e.m.). **c**, Left: Montage with overlaid tracks highlighting MreB movement in HC546(attλHC897) (Δ*ponA* Δ*pbpC* Δ*mtgA* ^{MS}*ponB* (P$_{lac}$::*mreB*-^{SW}*mNeon*)) after 30 min MTSES inactivation of PBP1b showing continuing MreB motion. Frames are 2 s apart. Scale bar = 1 μm. Original time-lapse movies are 1 s per frame. Right: Kymographs drawn along trajectories indicated on the phase contrast images (1, 2 and 3, left to right). Each tracked particle is highlighted with a coloured trajectory with the colour of the track (blue to red) indicating the passage of time. **d**, Distribution of velocities of MreB motion taken at different points after aPBP inhibition with MTSES (1 mM). For the tracks for which we can accurately calculate a particle's velocity, the fraction of moving particles only declines slightly (from 76 to 66%) during the time course following MTSES treatment. Microscopy results are representative of at least two independent experiments.

© 2016 Macmillan Publishers Limited, part of Springer Nature. All rights reserved.

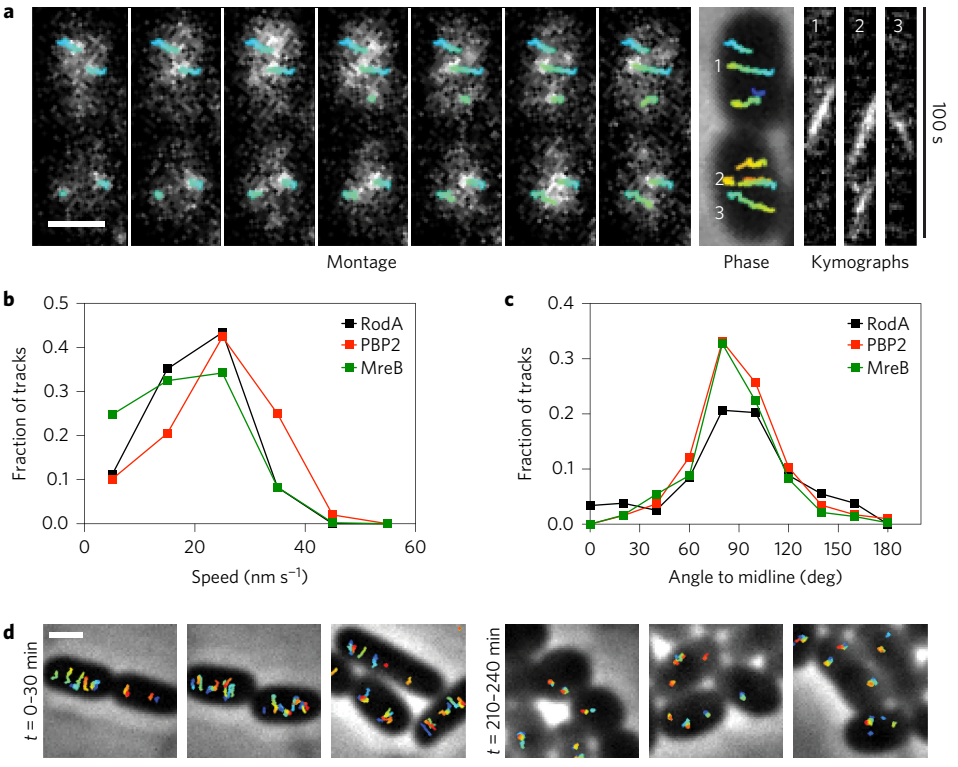

Figure 3 | PBP2 and RodA display directed, circumferential motions similar to MreB. a, Left to right: Montage of PBP2 movement with overlaid tracks in HC596(attHKHC943) (Δ*ponA* Δ*pbpC* Δ*mtgA* Δ*pbpA* (P_{lac}::*msfgfp-pbpA*)). Frames are 2 s apart. Each tracked particle is highlighted with a coloured trajectory as in Fig. 2c. Trajectories 1, 2 and 3 in the kymographs are in order from left to right. **b**, Distribution of velocities of tracked particles of MreB ($n = 807$), PBP2 ($n = 1{,}234$) and RodA ($n = 243$). **c**, Distribution of angles of PBP2 and RodA trajectories relative to the cell midline. **d**, Tracked particles of MreB-^{SW}mNeon at 0–30 or 210–240 min after induction of RodA(D262N) from strain TB28(attHKHC929)/pHC938 (WT(P_{tetA}::*mreB*-^{SW}*mNeon*)/P_{lac}::*pbpA-rodA*(*D262N*)). Each tracked particle is highlighted with a different coloured trajectory overlaid on a phase contrast image. Scale bars, 1 μm. In all cases, original time-lapse movies are 1 s per frame. Microscopy results are representative of at least two independent experiments.

display MreB-like circumferential motion, as has been observed in *B. subtilis*[5]. Imaging of a mostly functional sfGFP-RodA fusion (Supplementary Fig. 4a,b) revealed both fast, non-directionally moving particles consistent with molecules diffusing in the membrane and particles moving slowly and directionally at the same rate and angle as MreB (Fig. 3, Supplementary Fig. 5 and Supplementary Video 2). SEDS-family proteins form complexes with partner bPBPs (refs 1, 19 and 20), suggesting that RodA is likely to function in conjunction with PBP2. We therefore also investigated PBP2 dynamics using a functional msfGFP-PBP2 fusion (Supplementary Fig. 4a,c,d and Supplementary Video 3). Imaging at fast acquisition rates (50 or 100 ms per frame) showed what appeared to be particles rapidly diffusing within the membrane, as reported previously[21] (Supplementary Video 4). However, imaging with longer acquisition times (1 s per frame), which blurs the motion of rapidly diffusing particles across many pixels, revealed a subpopulation of PBP2 foci moving slowly and directionally around the cell circumference at the same rate and angle as MreB and RodA (Fig. 3, Supplementary Fig. 6 and Supplementary Video 4). These two types of PBP2 motion are analogous to what has been observed in *B. subtilis* for PBP2a (ref. 4). Similarly, we interpret the slow, rotating particles of RodA and PBP2 as those engaged in active, MreB-associated PG synthesis. To investigate whether RodA PGT activity is required for MreB motion, we monitored the effect of a dominant-negative RodA variant (D262N) (Supplementary Fig. 7) on MreB-^{SW}mNeon dynamics. This RodA derivative contains an amino acid change in a periplasmic loop residue critical for PGT activity[18]. Strikingly, production of RodA(D262N) but not RodA(WT) led to a gradual, filament-by-filament cessation of MreB-^{SW}mNeon motion (Fig. 3d and Supplementary Video 5). We therefore infer that RodA and PBP2 function as the core PGT/TP pair of the Rod system in both *E. coli* and *B. subtilis*[18].

aPBPs function outside of cytoskeletal complexes

In current models of PG biogenesis, aPBPs are associated with either the MreB- or FtsZ-directed synthetic machineries[1], implying that they function primarily within these complexes and may require cytoskeletal association for activity. However, cell growth and cell wall synthesis by an uncharacterized activity was previously observed in cells blocked for both FtsZ and MreB function[22,23], suggesting a possible cytoskeleton-independent mode of PG synthesis. Indeed, when PG synthesis and turnover were measured in HC533 cells blocked for both FtsZ and MreB activity by SulA and A22, respectively, significant PGT activity was still detected (Fig. 2a, sample 5). This activity was completely inhibited following MTSES treatment to inactivate ^{MS}PBP1b, indicating that cytoskeleton-independent synthesis is mediated by aPBPs (Fig. 2a, sample 7). To further test the dependence of aPBP polymerase activity on cytoskeletal function, we employed the aPBP-specific β-lactam cefsulodin[24], which induces increased glycan degradation similar to mecillinam[15]. This turnover probably reflects PGT activity promoted by aPBP molecules with drug-inactivated TP active sites (Fig. 1b). Consistent with this interpretation, treatment of ^{MS}PBP1b-producing (HC533) cells with MTSES completely blocked cefsulodin-induced glycan degradation (Fig. 4a,b: sample 1 versus 3; sample 2 versus 4). This result also supports the conclusion that ^{MS}PBP1b PGT activity is completely inactivated upon MTSES treatment. In contrast to MTSES addition, cefsulodin-induced turnover was stimulated by MreB depolymerization with

© 2016 Macmillan Publishers Limited, part of Springer Nature. All rights reserved.

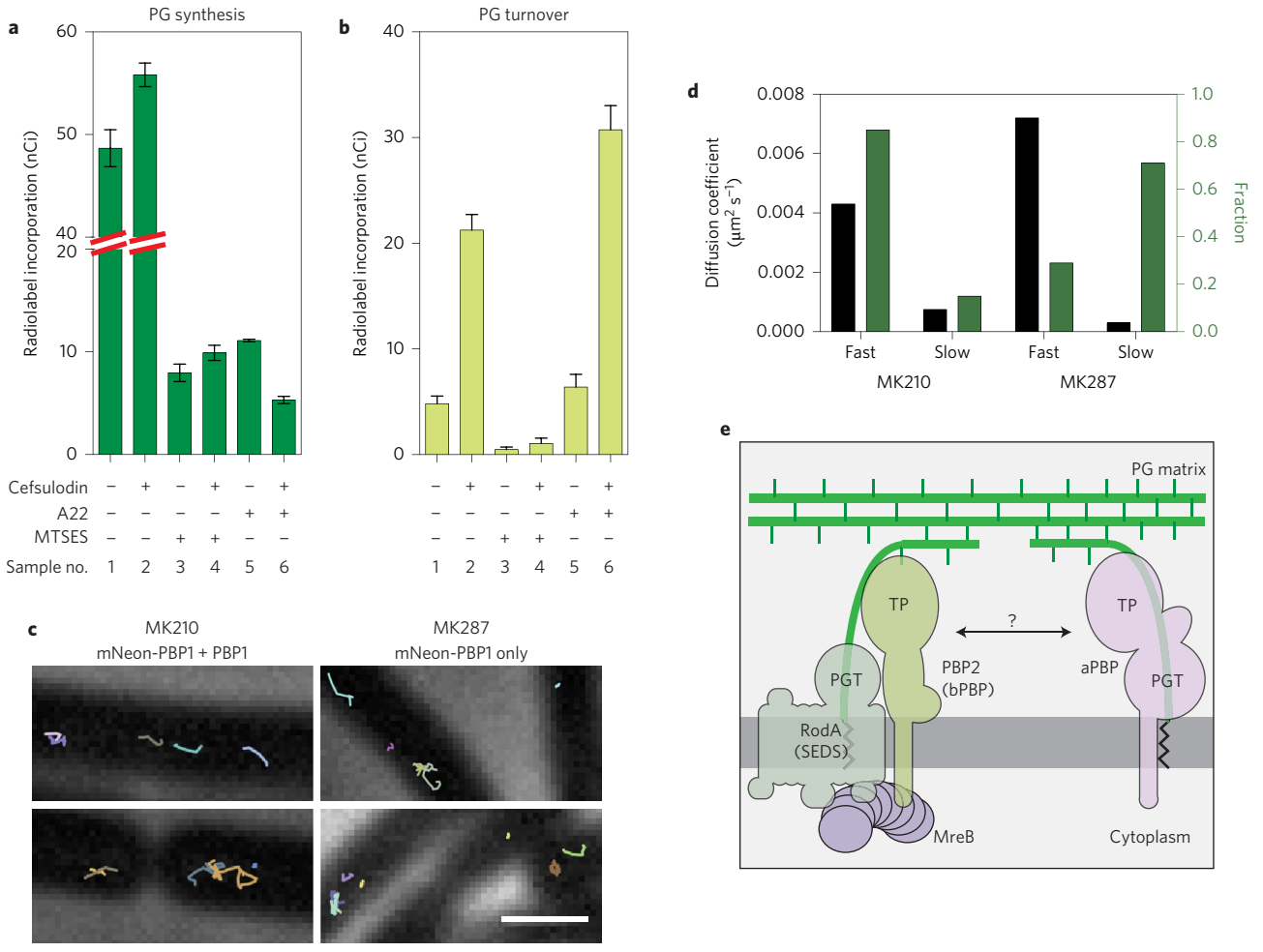

Figure 4 | aPBPs can function independently from the cytoskeletal machinery. a,**b**, PG matrix assembly and turnover were measured as in Fig. 2 using strain HC533(attλC739) (Δ*lysA* Δ*ampD* Δ*ponA* Δ*pbpC* Δ*mtgA* ^{MS}*ponB* (P_{tac}::*sulA*)). Cefsulodin was used at 100 μg ml^{-1}. Results are the average of three independent experiments. Error bars represent s.e.m. **c**, Tracks of mNeon-PBP1 expressed as (right) the only copy or (left) in addition to native untagged protein in *B. subtilis*. Each continuously tracked particle is highlighted with a different coloured trajectory. Note that although no MreB-like directional motion was observed, particles occasionally travel rapidly in one direction for a few frames, as expected for membrane diffusion. **d**, Graph showing diffusion constants and fraction of particles tracked in each diffusion state as determined by CDF analysis. Microscopy results are representative of at least two independent experiments. **e**, Schematic view of a new model for PG biogenesis involving two different classes of PG polymerases working semi-autonomously. SEDS PGTs and partner bPBPs perform PG polymerization and crosslinking in the context of the Rod system and divisome (not shown) while aPBPs function outside these complexes. Collaboration between the synthases probably occurs, but the mechanism remains to be defined.

A22 in cells already blocked for FtsZ activity by SulA (Fig. 4a,b, sample 5–6). Thus, glycan synthesis by PBP1b proceeds robustly in cells lacking all functional cytoskeletal filaments. Similarly, PG synthesis and turnover assays using cefsulodin and a strain where PBP1a was the sole remaining aPBP also detected cytoskeleton-independent glycan polymerization by PBP1a (Supplementary Fig. 8). The functionality of aPBPs in the absence of cytoskeletal filaments suggests that aPBPs may operate in a spatially distinct manner from the MreB- and FtsZ-directed machineries. To investigate this possibility, we followed aPBP subcellular dynamics in both *E. coli* and *B. subtilis*. In *E. coli*, a functional msfGFP-PBP1b (Supplementary Fig. 9) was produced as the sole aPBP. At the lowest induction level capable of supporting growth (13 μM), imaging at both long (1 s) and short (100 ms) acquisition times (like those used for PBP2 and RodA) did not reveal any directional motion (Supplementary Video 6a). We verified this result using single-molecule imaging of a functional Halo-tagged PBP1b fusion (Halo-PBP1b) labelled with low concentrations of JF-549 (ref. 25) (Supplementary Video 6b). Only motion consistent with membrane diffusion was observed. Similarly, imaging msfGFP-PBP1b motion during its depletion also did not reveal any MreB-like directional motion, even under conditions where depletion resulted in cell lysis. Furthermore, an msfGFP-PBP1a fusion produced as the sole aPBP in the cell also did not display MreB-like dynamics (Supplementary Video 7).

To determine whether aPBPs also display dynamics distinct from the Rod system in Gram-positive bacteria, we imaged a functional mNeon-PBP1 fusion (Supplementary Fig. 10) produced in *B. subtilis* as the sole copy of PBP1 or alongside the native protein. No directional motion was observed either when the fusion was produced from its native promoter or at low levels that allowed single molecule tracking (Fig. 4c,d, Supplementary Fig. 11 and Supplementary Videos 8–10). Rather, analysis of single-molecule trajectories using cumulative distribution functions (CDFs)[26,27] indicated that PBP1 exists in two states: diffusive (diffusion coefficient (D) = 0.004–0.007 μm^2 s^{-1}) and immobile (D = 0.0003–0.0007 μm^2 s^{-1}) (Fig. 4c,d, Supplementary Fig. 11 and Supplementary Videos 8–10). The slow, immobile particles predominated in cells producing mNeon-PBP1 as the sole source of PBP1 (Supplementary Video 9). When the fusion was expressed in addition to native PBP1, the fraction

© 2016 Macmillan Publishers Limited, part of Springer Nature. All rights reserved.

of faster diffusing molecules increased (Supplementary Video 10). This observation suggests a saturable number of available sites for the immobile particles that may reflect a functional state of PBP1. We conclude that aPBP polymerases from two different and evolutionarily distant model organisms display *in vivo* dynamics distinct from the circumferential motions observed for Rod system components.

A new view of PG biogenesis in bacteria

Overall, our results indicate that the aPBPs are not essential components of the Rod system in *E. coli* and suggest that these enzymes are performing significant roles in PG biogenesis apart from the complex. Instead of the aPBPs, the SEDS-protein RodA appears to supply the PG polymerase activity crucial for Rod system function[18]. The RodA polymerase, in turn, probably works in complex with PBP2, which provides crosslinking activity. By extension, the SEDS-family FtsW protein and its partner PBP3 are probably providing PG polymerase and crosslinking activity within the divisome. These findings necessitate a fundamental change in our view of the mechanism of cell wall assembly in bacteria and furthermore raise intriguing questions about the relative roles of the different types of PG polymerases in the process (Fig. 4e).

Inactivation of aPBP activity reduces total cell wall synthesis to approximately 20% of normal levels, indicating that these enzymes play major roles in PG biogenesis. The same is true when the cytoskeletal systems are inactivated and aPBPs remain functional; only about 20–30% of normal PG synthesis activity is detected. Thus, even though the aPBPs and Rod system components show distinct subcellular dynamics and are unlikely to be working stably together within the same complex, full cell wall synthesis efficiency requires that both systems be functional. Therefore, although our data support the idea that there is a division of labour between the aPBPs and the cytoskeleton-directed SEDS/bPBP systems, they appear to be only semi-autonomous and are probably collaborating with each other at some level. This partial interdependence may indicate that the two systems specialize in distinct but related aspects of the wall biogenesis process, similar to how different DNA polymerases work together to properly complete chromosome replication. For example, the more broadly conserved SEDS/bPBP systems[18] may build the primary structural foundation for the PG matrix, while the aPBPs support this foundation by adding to it and filling in gaps that arise during normal expansion and/or as the result of damage. Testing this and other possibilities in the context of the new framework provided in this and our companion report[18] will pave the way for a better mechanistic understanding of bacterial cell wall assembly and the discovery of novel ways to disrupt this process for antibiotic development.

Methods

Media, bacterial strains, plasmids and culture conditions for *E. coli* strains. Cells were grown in lysogeny broth (LB) (1% tryptone, 0.5% yeast extract, 0.5% NaCl) or minimal M9 medium supplemented with 0.2% casamino acids (CAA) and a carbon source (0.4% glycerol or 0.2% glucose or maltose), as indicated. The bacterial strains and plasmids used in this study are listed in Supplementary Tables 2 and 3, respectively, and a description of their construction is given in the following sections.

Construction of *E. coli* strains with multiple deletions. *E. coli* strains with multiple deletion mutations were made by sequential introduction of each deletion from the Keio mutant collection[28] via P1 transduction followed by removal of the *aph* cassette using FLP expressed from pCP20, leaving a *frt* scar sequence at each deletion locus. Correct orientation of the DNA flanking *frt* sequences in multiple deletion mutants was confirmed for all deletions in each mutant.

Construction of an MTSES-sensitive *E. coli* PBP1b variant. To test the effect of aPBP inhibition on cell wall synthesis and turnover, we sought a way to rapidly block the PGT activity of aPBPs. Moenomycin, a known inhibitor of the PGT activity of aPBPs, is not ideal for aPBP inhibition in WT *E. coli* because it cannot cross the outer membrane layer to access aPBPs. Instead, it was recently shown that a small cysteine-reactive molecule, MTSES, can be used in conjunction with a cysteine-substitution mutant to specifically block the activity of a surface exposed enzyme[17]. PBP1B was chosen for the development of an MTSES-blockable aPBP system because it is the major aPBP in *E. coli*, and structural information was also available for this protein[29]. Thirteen cysteine substitution variants of PBP1b were constructed with changes mapping within the moenomycin binding surface of PBP1B (ref. 28). Alleles encoding each variant were cloned under control of the *lac* promoter in the CRIM plasmid pHC872 backbone (*attHK022*, P_{lac}::*ponB*) and the resulting plasmids were integrated into HC518 (⊗*ponA*::*frt* P_{ara}::*ponB*). The functionality of each *ponB* allele was assessed by testing their ability to correct the PBP1a– PBP1b– synthetic lethality of HC518 grown on M9 glucose minimal medium supplemented with 100 μM isopropyl β-D-1-thiogalactopyranoside (IPTG).

Cysteine substitution mutants that were functional were further screened for loss of activity following MTSES treatment. This screen used the rapid lysis phenotype manifested in cells inhibited for aPBP activity in combination with 10 μg ml^{-1} cephalexin.

Treatment of WT *E. coli* with 10 μg ml^{-1} cephalexin causes continued growth as cell filaments. However, lysis is observed in 20 min when aPBPs are also inhibited. We therefore screened the functional PBP1b cysteine substitution mutants for their response to treatment with 10 μg ml^{-1} cephalexin with or without 1 mM MTSES using a VersaMax microplate reader (Molecular Devices). PBP1b(S247C) was identified as a variant that supports the growth, similar to WT PBP1b, but specifically leads to rapid lysis when cells producing the variant as the main aPBP are treated with 10 μg ml^{-1} cephalexin and 1 mM MTSES.

Introducing *ponB*(*S247C*) mutation at the native *E. coli* locus. Allele exchange of *ponB*(*247C*) at the native locus was performed using a temperature-sensitive plasmid pMAK700, as described in ref. 30. A total of 1,800 bases of DNA flanking the *ponB*(*S247C*) mutation were PCR-amplified from pHC873 using primers 5′-GCTA*ATCGAT*GAAAATCGGGGCTTTTGCGCCTGAATATTGC-3′ and 5′- GCTA*GCTAGC*AGATTTACCGTCGGCACGTTCATCG-3′. The resulting PCR product was digested with NheI and ClaI and ligated with pMAK700 digested with the same enzymes to generate pHC878. Plasmid integration and excision events at the *ponB* locus were selected using the temperature-sensitive replication initiation of pHC878 to obtain strains with *ponB*(*S247C*) mutation at the native chromosomal locus.

Introduction of the *imp4213* allele. The *imp4213* allele was introduced into recipient strains by P1 transduction using its genetic linkage to the *leu* marker. First, a *leu*::*Tn10* marker was introduced into the recipient strains by selecting for tetracycline resistance. Then, *imp4213* was introduced into the *leu* auxotrophs by P1 transduction followed by selection for leucine prototrophy on M9–glucose agar plates. For efficient P1 lysate preparation from an *imp4213* strain, a strain that has a suppressor mutation at the *bamA* locus in addition to *imp4213* (JAB027) was used. The resulting P1 transductants were screened for sensitivity to 10 μg ml^{-1} erythromycin to identify isolates that acquired the *imp4213* allele together with the WT *leu* locus.

Generation of *mreB* sandwich fusions at the native *E. coli mre* locus. Sandwich fluorescent protein fusions of *mreB* were introduced at the native locus using the recombineering strain CH138/pCX16, which harbours a defective lambda prophage as a temperature-inducible source of the recombination genes[31]. CH138/pCX16 is also deleted for native *galK* and has a *galK* cassette inserted in the middle of *mreB* (replacing the codon for G228). The strain is viable due to suppression of the Rod system defect by elevated FtsZ levels promoted by *sdiA* on pCX16. Fragments with 1 kb of sequence flanking *mNeonGreen* or *mCherry* in plasmid-borne *mreB*-fluorescent protein sandwich fusions were amplified with primers 5′-AACGGTGTGGTTTACTCCTCTTCTGTG-3′ and 5′-TTCCAGTGCAACCATTACCGCGCTCAC-3′ using pFB262 or pHC892 as templates. After recombineering with the resulting PCR products, cells that replaced *galK* with fluorescent protein fusions at the *mreB* locus were selected on M9 minimal agar containing 0.2% 2-deoxy-galactose, which is converted to toxic 2-deoxy-galactose-1-phosphate if cells remain GalK+.

Generation of *E. coli ΔrodA::aph*. A *rodA* deletion was constructed in a manner similar to deletions in the Keio collection[28] using a TB10(attHKCS8) recombineering strain that expresses *rodA* under control of the *lac* promoter. A PCR product for *ΔrodA*::*aph* construction was amplified using pKD13 (ref. 32) as a template with primers 5′-AAAATCCAGCGGTTGCCGCAGCGGAGGACCA TTAATCATGATTCCGGGGATCCGTCGACC-3′ and 5′-CTTACGCATTGCGCA CCTCTTACACGCTTTTCGACAACATTGTAGGCTGGAGCTGCTTCG-3′ and recombineering was performed as described previously[33].

E. coli plasmid construction

pHC872 and pHC873. The *ponB* gene was amplified with primers 5′-GTCA*TCTAGA* GAAAATCGGGCTTTTGCGCCTG-3′ and 5′-GTCA*CTCGAG*ATGGGATGTTA TTTTACCGGATGGC-3′. The resulting fragment was digested with XbaI and XhoI and ligated to pTB183 digested with XbaI and SalI to generate pMM15. The *bla* antibiotic resistance cassette of pMM15 was replaced with a *cat* cassette from pHC514 by replacing the NotI-XbaI fragment to generate pHC872. The *ponB* (*S247C*) mutation was introduced in pHC872 using QuikChange mutagenesis with the primer 5′-CATGATGGAATCAGTCTCTACTGCATCGGA CGTGCGGTGCTGGCA-3′ to generate pHC873.

© 2016 Macmillan Publishers Limited, part of Springer Nature. All rights reserved.

pHC897. The *mCherry* sequence of pFB262 was replaced with *E. coli* codon-optimized *mNeonGreen* (IDT synthesis) using XhoI and AscI to generate pHC892. The *mreB-*^{SW}*mNeon* fragment of pHC892 was removed with XbaI and HindIII and cloned under control of the *lac* promoter of a pHC514 derivative to generate pHC897.

pHC929. The *mreB-*^{SW}*mNeon* fragment was liberated from pHC892 by digestion with XbaI and HindIII, and *tetR*-P_{tetA} (Integrated DNA Technologies synthesis) digested with BglI and XbaI was assembled in a pTB183 derivative using BglII and HindIII to generate pHC929.

pHC938. pHC938 was generated by introducing the *rodA*(*D262N*) mutation into pHC857 using an overlap extension mutagenesis protocol. *rodA*(*D262N*) was amplified using primers 5′-AAATCC*GGTACC*GCTCAGGTC-3′ and 5′-GTA TCGGTGAT*AAGCTT*CTGC-3′ and a mutagenizing primer set 5′-CCGAACGCCA TACT**A**AC**T**TTATCTTCGCGGTACTGG-3′ and 5′-GCGAAGATAAAGT**T**AGTA TGGCGTTCGGGGAGAAATTC-3′. The mutated base is indicated in bold. The resulting PCR product for *rodA*(*D262N*) was digested with KpnI and HindIII and ligated to pHC857 digested with the same enzymes to generate pHC938.

pHC933. The *sfgfp* fragment was liberated from pTB230 with XbaI and BamHI digestion and *rodA* amplified with 5′-GTCA*GGATCC*GAGGCCATTACGGCCA TGACGGATAATCCGAATAAAAAAACATTCTGGG-3′ and 5′-GTCA*GTCGA CTTATTATTGGCCGAGGCGGCCTTACACGCTTTTC-3′ and digested with BamHI and SalI. The fragments were assembled in pNP20 using XbaI and SalI to generate pHC933.

pHC942, pHC943 and pPR104. E. coli codon-optimized *msfgfp* (IDT synthesis) digested with XbaI and BamHI, and the *ponB* sequence amplified with 5′-GTA C*GGATCC*CCGCGCAAAGGTAAGGG-3′ and 5′-GTCA*CTCGAG*ATGGGA TGTTATTTTACCGGATGGC-3′ and digested with BamHI and XhoI were assembled in pNP20 by using XbaI and SalI to generate pHC942. The *ponB* of pHC942 was then replaced with *pbpA* sequence amplified with 5′-GCTA*GGA TCC*AAACTACAGAACTCTTTTCGCGACTATACG-3′ and 5′-CTTCA CGTTCGCTCGCGTATCGGTG-3′ using BamHI and HindIII to generate pHC943. pPR104 was constructed by replacing *ponB* of pHC942 with *ponA* sequence amplified with 5′-GCTA*GGATCC*AAGTTCGTAAAGTATTTTTTGATCC-3′ and 5′-GCTA*AAGCTT*AGAACAATTCCTGTGCCTCGCCAT-3′ using BamHI and HindIII.

pHC949. The *HaloTag* sequence was amplified using pDHL940 as a template with 5′-GCTA*TCTAGA*ATTTAAGAAGGAGATATACATATGGCAGAAATCGGTA CTGGCTTTCCATTC-3′ and 5′-GCTA*GGATCC*GGAAATCTCCAGAGTAGACA GC-3′. The resulting PCR product was digested with XbaI and BamHI and ligated to pHC942 digested with the same enzymes to replace the *msfgfp* sequence with *HaloTag* sequence.

Measurement of PG synthesis and turnover. The effect of blocking aPBP activity with MTSES on PG synthesis and turnover in β-lactam-treated *E. coli* cells was examined essentially as described previously[15]. HC533(attλHC739), a *ΔlysA ΔampD* strain that expresses PBP1b(S247C) as a sole aPBP, was grown overnight in M9-glycerol medium supplemented with 0.2% CAA. The overnight culture was diluted to an optical density at 600 nm (OD_{600}) of 0.04 in the same medium and grown to an OD_{600} of between 0.26 and 0.3. Divisome formation was then blocked by inducing *sulA* expression for 30 min from a chromosomally integrated P_{tac}::*sulA* construct (pHC739) by adding IPTG to 1 mM. After adjusting the culture OD_{600} to 0.3, MTSES (1 mM), A22 (10 μg ml^{-1}), mecillinam (10 μg ml^{-1}) and/or cefsulodin (100 μg ml^{-1}) were added to the final concentrations indicated and cells were incubated for 5 min. Following drug treatment, 1 μCi of [^{3}H]-meso-2,6-diaminopimelic acid (mDAP) was added to 1 ml of each drug-treated culture and incubated for 10 min to label the newly synthesized PG and its turnover products. After labelling, cells were pelleted, resuspended in 0.7 ml water, and heated at 90 °C for 30 min to extract water-soluble compounds. After hot water extraction, insoluble material was pelleted by ultracentrifugation (200,000*g* for 20 min at 4 °C). The resulting supernatant was then removed, lyophilized and resuspended in 0.1% formic acid for HPLC analysis and quantification of turnover products as described previously[15]. To determine the [^{3}H]-mDAP incorporated into the PG matrix, the pellet fraction was washed with 0.7 ml buffer A (20 mM Tris-HCl, pH 7.4, 25 mM NaCl) and resuspended in 0.5 ml buffer A containing 0.25 mg lysozyme. The suspensions were incubated overnight at 37 °C. Insoluble material was then pelleted by centrifugation (21,000*g* for 30 min at 4 °C) and the resulting supernatant was mixed with 10 ml EcoLite (MP Biomedicals) scintillation fluid and quantified in a Microbeta Trilux 1450 liquid scintillation counter (Perkin-Elmer).

Quantification of MTSES labelling of PBP1b(S247C). To quantify the efficiency of MTSES binding to PBP1b(S247C) under experimental growth conditions, a culture of HC533(attλHC739) (100 ml) was grown to an OD_{600} of 0.3 in M9-glycerol medium supplemented with 0.2% CAA at 30 °C with *sulA* induction for 30 min. The culture was then split into two 50 ml portions and treated with either 1 mM MTSES or dimethylsulfoxide (DMSO) for 5 min. Immediately after MTSES/DMSO treatment, cultures were cooled on ice and cells were pelleted at 4,000*g* for 5 min at 4 °C. The cell pellets were washed once with 1× ice-cold phosphate-buffered saline (PBS), resuspended in 500 μl 1× PBS containing 10 mM EDTA and 20 mM 2-iodoacetamide, and incubated for 20 min at room temperature to alkylate the cysteine residues not modified by MTSES. After 20 min incubation, 20 kU of Ready-lyse lysozyme (Epicentre) was added to each cell suspension, and incubation was continued for a further 10 min at room temperature. Cells were disrupted by sonication, and membrane fractions were pelleted by ultracentrifugation at 200,000*g* for 20 min at 4 °C. The membrane fractions were then washed with 1× PBS once, and resuspended in 1 ml immunoprecipitation (IP) buffer (100 mM Tris, pH 7.4, 300 mM NaCl, 2% Triton X-100). Anti-PBP1b antiserum (10 μm) was added to the resuspension, and the resuspension was incubated overnight in the cold room with gentle agitation. The samples were then mixed with 50 μl of IP buffer-equilibrated protein A/G magnetic beads (Millipore) and incubated for a further 4 h in the cold room with gentle agitation. The beads were then washed three times with IP buffer and then three times with a buffer containing 100 mM Tris, pH 7.4 and 300 mM NaCl.

Proteins bound on the beads were fragmented by on-bead digestion with 0.1 μg trypsin (#V511C, Promega) in 300 μl buffer (20 mM Tris-HCl, pH 8, 150 mM NaCl) overnight at 37 °C with gentle agitation. After digestion, peptide samples were acidified with 10% trifluoroacetic acid (TFA) to a pH between 1 and 2, desalted using a 96-well plate embedded with C18 resin (Thermo Scientific) and dried by vacuum centrifugation. Samples were resolubilized in 20 μl of 0.1% TFA and 5 μl of each sample was analysed by nanoscale liquid chromatography coupled to tandem mass spectrometry (ref. 34) with an HPLC gradient (NanoAcquity UPLC system, Waters; 5–35% B in 110 min; A = 0.1% formic acid in water, B = 0.1% formic acid in acetonitrile). Peptides were resolved on a self-packed analytical column (50 cm Monitor C18, Column Engineering) and introduced to the mass spectrometer (Q Exactive HF) at a flow rate of 30 nl min^{-1} (electrospray ionization spray voltage = 3.5 kV). The mass spectrometer was programmed to operate in data-dependent mode such that the ten most abundant precursors in each full MS scan (resolution = 120 K; target = 5e5; maximum injection time = 500 ms; scan range = 300–2,000 *m*/*z*) were subjected to high-energy collisional dissociation (resolution = 15 K; target = 5e4; maximum injection time = 200 ms; isolation window = 1.6 *m*/*z*; Normalized collision energy = 27, 30; dynamic exclusion = 15 s). MS/MS spectra were matched to peptide sequences using Mascot (version 2.2.1) after conversion of raw data to .mgf using multiplierz scripts[35]. Search parameters specified trypsin digestion with up to two missed cleavages, as well as variable oxidation of methionine and carbamidomethylation of cysteine residues. Precursor and product ion tolerances were 10 ppm and 25 milli mass units, respectively. Targeted scan experiments were performed in a similar fashion while dynamic exclusion was disabled and inclusion was enabled for the following peptides: HFYEHDGISLYCIGR (carbamidomethyl cysteine: *z* = 4, *m*/*z* = 467.4703; *z* = 3, *m*/*z* = 622.9579; *z* = 2, *m*/*z* = 933.9332), HFYEHDGISLYCIGR (MTSES-cysteine: *z* = 4, *m*/*z* = 488.2050; *z* = 3, *m*/*z* = 650.6042; *z* = 2, *m*/*z* = 975.4026), VWQLPAAVYGR (*z* = 2, *m*/*z* = 630.3484), LLEATQYR (*z* = 2, *m*/*z* = 497.2718), QFGFFR (*z* = 2, *m*/*z* = 401.2058), DSDGVAGWIK (*z* = 2, *m*/*z* = 524.2589). Peak area integration was carried out using the Thermo Xcalibur Qual Browser (version 3.0.63, Thermo Fisher Scientific).

Bocillin-binding assays. Cultures of HC545, HC596(attHKHC943) and HC576 (attHKHC942) were grown overnight at 37 °C in M9-glucose medium supplemented with 0.2% CAA, with induction of *msfgfp-pbpA* or *msfgfp-ponB* with 25 μM IPTG. Cells in the overnight cultures were washed to remove IPTG and diluted to an OD_{600} of 0.001 in 15 ml of M9-glucose medium supplemented with 0.2% CAA and the indicated concentrations of IPTG. The cultures were then incubated at 37 °C until the OD_{600} reached 0.4–0.5. A subset of cultures were treated with 10 μg ml^{-1} mecillinam (specific for PBP2) or 100 μg ml^{-1} cefsulodin (specific for PBP1b) for 5 min before harvesting. Cells were then collected by centrifugation at 4 °C, washed with ice-cold 1× PBS twice, resuspended in 500 μl 1× PBS containing 10 mM EDTA and 15 μM Bocillin (Invitrogen) and incubated at room temperature for 15 min. After incubation, the cell suspensions were washed with 1× PBS once, resuspended in 500 μl 1× PBS and disrupted by sonication. After a brief spin for 1 min at 4,000*g* to remove undisrupted cells, membrane fractions were pelleted by ultracentrifugation at 200,000*g* for 20 min at 4 °C. The membrane fractions were then washed with 1× PBS and resuspended in 50 μl 1× PBS. Resuspended samples were mixed with 50 μl 2× Laemmli sample buffer and boiled for 10 min at 95 °C. After measuring the total protein concentrations of each sample with NI-protein assay (G-Biosciences), 25 μg of total protein for each sample was then separated on a 10% SDS–polyacrylamide gel electrophoresis (PAGE) gel and the labelled proteins were visualized using a Typhoon 9500 fluorescence imager (GE Healthcare) with excitation at 488 nm and emission at 530 nm.

Bocillin-binding assays for *B. subtilis* strains were performed essentially in the same way as for *E. coli* strains. Overnight cultures grown in casein hydrolysate (CH) medium at room temperature were diluted to OD_{600} = 0.04–0.07 in 5 ml fresh CH medium containing the indicated concentrations of IPTG and incubated at 37 °C. When the cultures reached exponential phase, cells were pelleted, washed with ice-cold 1× PBS and resuspended with 100 μl 1× PBS containing 15 μM Bocillin (Invitrogen) and incubated for 15 min at room temperature. The cells were then washed in 1× PBS, resuspended 0.5 ml 1× PBS containing 20 kU Ready-lyse lysozyme (Epicentre) and incubated for 15 min at room temperature. The cells were

© 2016 Macmillan Publishers Limited, part of Springer Nature. All rights reserved.

disrupted by sonication and the membrane fraction was isolated by ultracentrifugation. A total of 16 µg of protein for each sample was separated on a 10% SDS–PAGE gel and visualized as described for *E. coli*.

Microscopy of *E. coli* cells. Overnight cultures with strain-specific inducer levels were diluted in fresh culture medium and grown for at least 3 h at 37 °C to an OD_{600} below 0.6. Cells were concentrated by centrifugation at 7,200*g* for 3 min and applied to No. 1.5 cover glass under 5% agarose pads with culture medium, except for microscopy with MTSES, which was performed using the CellASIC ONIX microfluidic platform from EMD Millipore.

For msfGFP-PBP2 tracking, M9-glucose-CAA medium was used with 25 µM IPTG. For sfGFP-RodA tracking, M9-maltose-CAA medium was used with 80 µM IPTG. For msfGFP-PBP1b imaging, M9-glucose-CAA medium was used with a starting concentration of 20 µM IPTG, diluted to 13 µM final IPTG before expansion at 37 °C. For MreB-^{SW}Neon tracking with MTSES-treated cells, M9-glucose-CAA medium was used with 100 µM. For Halo-PBP1b tracking, M9-glucose-CAA medium was used with 50 µM IPTG; before imaging cells were treated with 6.25 nM dye for 15 min.

For MreB-^{SW}mNeon tracking following RodA (WT) or RodA (D262N) overproduction, M9-maltose-CAA medium was used with the addition of 0.8 ng µl^{-1} anhydrotetracycline before growth at 37 °C. For experiments following the effect of RodA variant production after 210 min induction, cells were first grown in liquid culture for 120 min under inducing conditions (1 mM IPTG) before concentration and imaging. IPTG (1 mM) was included in the agarose pads used for imaging.

Microscopy of *B. subtilis* cells. Overnight cultures grown in CH medium were diluted in fresh medium and grown for at least 3 h at 37 °C to an OD_{600} below 0.3. Cells were concentrated by centrifugation at 6,000*g* for 30 s and applied to No. 1.5 cover glass under 2% agarose pads with CH medium. For PBP1 imaging, no inducer was added to the cultures; leaky expression of mNeonGreen-PBP1 was sufficient for particle tracking experiments. All cells were imaged at 37 °C under an agar pad with the top surface exposed to air.

For measurements of growth rate, overnight cultures grown in LB medium were diluted in fresh medium and grown for at least 3 h at 37 °C and to an OD_{600} below 0.3. The culture was diluted to an OD_{600} of 0.07 and its growth curve was measured in a Growth Curves USA Bioscreen-C Automated Growth Curve Analysis System.

For measurements of cell widths, overnight cultures grown in CH medium were diluted in fresh medium (with addition of 10 µM IPTG where indicated) for at least 3 h at 37 °C and to an OD_{600} below 0.3. Cells were stained with FM 5–95 (ThermoFisher Scientific) and imaged under agarose pads as described above.

Particle tracking microscopy. Total internal reflection fluorescence microscopy (TIRF-M) and phase contrast microscopy were performed using a Nikon Eclipse Ti equipped with a Nikon Plan Apo λ 100× 1.45 objective and a Hamamatsu ORCA-Flash4.0 V2 (C11440-22CU) sCMOS camera. Except where specified, fluorescence time-lapse images were collected by continuous acquisition with 1,000 ms exposures. Microscopy was performed in a chamber heated to 37 °C.

Wide-field epifluorescence microscopy. Wide-field epifluorescence microscopy was performed on the instrument described above and, for some samples, on a DeltaVision Elite Microscope equipped with an Olympus 60× Plan Apo 60× 1.42 NA objective and a PCO.edge sCMOS camera. Cell contours and dimensions were calculated using the Morphometrics software package[36].

Particle tracking. Particle tracking was performed using the software package FIJI (refs 37,38) and the TrackMate plugin. For calculation of particle velocity, the scaling exponent α and track orientations relative to the midline of the cell, only tracks persisting for seven frames or longer were used. Particle velocity for each track was calculated from nonlinear least-squares fitting using the equation $MSD(t) = 4Dt + (vt)^2$, where MSD is the mean squared displacement, t is time interval, D is the diffusion coefficient and v is speed. The maximum time interval used was 80% of the track length. Tracks were excluded from further evaluation if the contribution of directional motion to the MSD was less than 0.01 nm s^{-1}. Tracks were also excluded if R^2 for log MSD versus log t was less than 0.9, indicating a poor ability to fit the MSD curve. For PBP2, R^2 and speed filtering together resulted in the exclusion of ~50% of detected tracks. Track overlays in figures include all tracks seven frames or longer to illustrate the performance of the track detection algorithms.

Track angles relative to the cell axis were taken to be the direction of the line produced by orthogonal least-squares regression using all of the points in each track; cell axis angles were determined by finding cell outlines and axes using the Morphometrics software package[36].

Analysis of PBP1 diffusion. Tracking of *B. subtilis* mNeon-PBP1 in strains MK210 and MK287 was performed using the u-track 2.0 software package[40]. Resulting trajectories were then manually filtered to minimize particle detection and linking errors. The frame-to-frame vector displacements along these trajectories were then calculated. The magnitude of each of the displacements was taken and the CDF of the pool of displacements across all movies in a condition was calculated. The CDF of the displacement magnitudes was then fit to an analytical function describing a diffusion process whereby one or more unique states of diffusion were occurring. The analytical form of the two-state model used in the results is:

$$P(r, \Delta t) = 1 - we^{-\left(\frac{r^2}{4D_1\Delta t}\right)} - (1-w)e^{-\left(\frac{r^2}{4D_2\Delta t}\right)}$$

where $P(r, \Delta t)$ is the cumulative probability of a displacement of magnitude r given the observation period Δt, diffusion coefficients D_1,D_2 and the relative fractions between those two states w. For a more simple, one-state model, $w = 1$.

The fitting was performed in MATLAB using a nonlinear least-squares algorithm with 500 restarts to the initial parameters so as to find a close approximation to the true parameters of the model. Residuals of the model fit were calculated and used in the determination of the number of distinct diffusive species present within the data set.

***B. subtilis* strain construction.** For MK005 [Δ*ponA*] construction, the homology region upstream of *ponA* was amplified from Py79 DNA using oligos oMK001 and oMK002. The *cat* cassette was amplified from pGL79 using oligos oJM28 and oJM29. The homology region downstream of *ponA* was amplified from Py79 DNA using oligos oMK006 and oMK013. The three fragments were fused using isothermal assembly[38] and transformed into Py79 to give MK005 by selecting on chloramphenicol agar.

For MK095, a native functional fusion of mNeonGreen to PBP1 was constructed by isothermal assembly[38] and was recombined into the chromosome of Py79 using counterselection to produce a marker-less strain without any remaining scars. The homology region upstream of *ponA*, fused to the first 30 bases of the coding sequence of mNeonGreen, was amplified from Py79 DNA using oMK001 and oMK027. The *cat* cassette, the P_{xyl} promoter sequence and the *mazF* coding sequence were amplified as a fused fragment from template DNA using primers oMK047 and oMK086. The coding sequence of mNeonGreen was amplified from a gBlock using primers oMK078 and oMK087. The downstream homology region encoding a portion of the PBP1 (*ponA*) coding sequence was amplified from Py79 DNA using oMK009 and oMK050. These fragments were fused using isothermal assembly and transformed into Py79 to give MK093 upon selection for chloramphenicol resistance. Because the primers oMK078 and oMK009 contained the sequence for a 15-amino-acid flexible linker, the fused product encoded an mNeonGreen-PBP1 fusion protein. The presence of a fragment of the mNeonGreen coding region upstream of *cat* provided a direct repeat to allow for spontaneous removal of the *cat-mazF* sequence by recombination. MK093 was grown in LB medium for 4 h to allow time for recombination, and 200 µl cells were plated on an LB plate containing 30 mM xylose. This selected for cells that removed the *cat-mazF*, yielding a scar-less functional fusion protein under control of the native PBP1 promoter.

Strains MK210 and MK287 encoding an inducible version of the mNeonGreen-PBP1 fusion protein were constructed by isothermal assembly. The homology region upstream of *amyE*, the *erm* cassette and the *LacI*-$P_{hyperspank}$ promoter construct were amplified as a fused fragment from template DNA using primers oMD191 and oMD232. The mNeonGreen-PBP1 coding sequence was amplified from MK095 DNA using primers oMK100 and oMK138. The homology region downstream of *amyE* was amplified from Py79 DNA using oMD196 and oMD197. The fragments were fused using isothermal assembly and transformed into Py79 to give MK210. Genomic DNA from MK005 (*ΔponA*::cat) was transformed into MK210 to give MK287, a strain in which the mNeonGreen-PBP1 fusion protein was the only copy of PBP1.

Received 16 July 2016; accepted 17 August 2016; published 19 September 2016

References

1. Typas, A., Banzhaf, M., Gross, C. A. & Vollmer, W. From the regulation of peptidoglycan synthesis to bacterial growth and morphology. *Nat. Rev. Microbiol.* **10,** 123–136 (2012).
2. McKenna, M. Antibiotic resistance: the last resort. *Nature* **499,** 394–396 (2013).
3. Jones, L. J., Carballido-López, R. & Errington, J. Control of cell shape in bacteria: helical, actin-like filaments in *Bacillus subtilis*. *Cell* **104,** 913–922 (2001).
4. Garner, E. C. *et al.* Coupled, circumferential motions of the cell wall synthesis machinery and MreB filaments in *B. subtilis*. *Science* **333,** 222–225 (2011).
5. Domínguez-Escobar, J. *et al.* Processive movement of MreB-associated cell wall biosynthetic complexes in bacteria. *Science* **333,** 225–228 (2011).
6. van Teeffelen, S. *et al.* The bacterial actin MreB rotates, and rotation depends on cell-wall assembly. *Proc. Natl Acad. Sci. USA* **108,** 15822–15827 (2011).
7. Ursell, T. S. *et al.* Rod-like bacterial shape is maintained by feedback between cell curvature and cytoskeletal localization. *Proc. Natl Acad. Sci. USA* **111,** E1025–E1034 (2014).
8. Bi, E. F. & Lutkenhaus, J. FtsZ ring structure associated with division in *Escherichia coli*. *Nature* **354,** 161–164 (1991).
9. Yousif, S. Y., Broome-Smith, J. K. & Spratt, B. G. Lysis of *Escherichia coli* by beta-lactam antibiotics: deletion analysis of the role of penicillin-binding proteins 1A and 1B. *J. Gen. Microbiol.* **131,** 2839–2845 (1985).

© 2016 Macmillan Publishers Limited, part of Springer Nature. All rights reserved.

10. Hoskins, J. *et al.* Gene disruption studies of penicillin-binding proteins 1a, 1b, and 2a in *Streptococcus pneumoniae*. *J. Bacteriol.* **181,** 6552–6555 (1999).
11. Paik, J., Kern, I., Lurz, R. & Hakenbeck, R. Mutational analysis of the *Streptococcus pneumoniae* bimodular class A penicillin-binding proteins. *J. Bacteriol.* **181,** 3852–3856 (1999).
12. Sauvage, E., Kerff, F., Terrak, M., Ayala, J. A. & Charlier, P. The penicillin-binding proteins: structure and role in peptidoglycan biosynthesis. *FEMS Microbiol. Rev.* **32,** 234–258 (2008).
13. McPherson, D. C. & Popham, D. L. Peptidoglycan synthesis in the absence of class A penicillin-binding proteins in *Bacillus subtilis*. *J. Bacteriol.* **185,** 1423–1431 (2003).
14. Rice, L. B. *et al.* Role of class A penicillin-binding proteins in the expression of beta-lactam resistance in *Enterococcus faecium*. *J. Bacteriol.* **191,** 3649–3656 (2009).
15. Cho, H., Uehara, T. & Bernhardt, T. G. Beta-lactam antibiotics induce a lethal malfunctioning of the bacterial cell wall synthesis machinery. *Cell* **159,** 1300–1311 (2014).
16. Uehara, T. & Park, J. T. Growth of *Escherichia coli*: significance of peptidoglycan degradation during elongation and septation. *J. Bacteriol.* **190,** 3914–3922 (2008).
17. Sham, L.-T. *et al.* Bacterial cell wall. MurJ is the flippase of lipid-linked precursors for peptidoglycan biogenesis. *Science* **345,** 220–222 (2014).
18. Meeske, A. J. *et al.* SEDS proteins are a widespread family of bacterial cell wall polymerases. *Nature* http://dx.doi.org/10.1038/nature19331 (2016).
19. Fay, A., Meyer, P. & Dworkin, J. Interactions between late-acting proteins required for peptidoglycan synthesis during sporulation. *J. Mol. Biol.* **399,** 547–561 (2010).
20. Fraipont, C. *et al.* The integral membrane FtsW protein and peptidoglycan synthase PBP3 form a subcomplex in *Escherichia coli*. *Microbiology* **157,** 251–259 (2011).
21. Lee, T. K. *et al.* A dynamically assembled cell wall synthesis machinery buffers cell growth. *Proc. Natl Acad. Sci. USA* **111,** 4554–4559 (2014).
22. Varma, A., de Pedro, M. A. & Young, K. D. FtsZ directs a second mode of peptidoglycan synthesis in *Escherichia coli*. *J. Bacteriol.* **189,** 5692–5704 (2007).
23. Tan, Q., Awano, N. & Inouye, M. YeeV is an *Escherichia coli* toxin that inhibits cell division by targeting the cytoskeleton proteins, FtsZ and MreB. *Mol. Microbiol.* **79,** 109–118 (2011).
24. Curtis, N. A., Orr, D., Ross, G. W. & Boulton, M. G. Affinities of penicillins and cephalosporins for the penicillin-binding proteins of *Escherichia coli* K-12 and their antibacterial activity. *Antimicrob. Agents Chemother.* **16,** 533–539 (1979).
25. Grimm, J. B. *et al.* A general method to improve fluorophores for live-cell and single-molecule microscopy. *Nat. Methods* **12,** 244–250 (2015).
26. Vrljic, M., Nishimura, S. Y., Brasselet, S., Moerner, W. E. & McConnell, H. M. Translational diffusion of individual class II MHC membrane proteins in cells. *Biophys. J.* **83,** 2681–2692 (2002).
27. Schütz, G. J., Schindler, H. & Schmidt, T. Single-molecule microscopy on model membranes reveals anomalous diffusion. *Biophys. J.* **73,** 1073–1080 (1997).
28. Baba, T. *et al.* Construction of *Escherichia coli* K-12 in-frame, single-gene knockout mutants: the Keio collection. *Mol. Syst. Biol.* **2,** 2006.0008 (2006).
29. Sung, M.-T. *et al.* Crystal structure of the membrane-bound bifunctional transglycosylase PBP1b from *Escherichia coli*. *Proc. Natl Acad. Sci. USA* **106,** 8824–8829 (2009).
30. Cho, H., McManus, H. R., Dove, S. L. & Bernhardt, T. G. Nucleoid occlusion factor SlmA is a DNA-activated FtsZ polymerization antagonist. *Proc. Natl Acad. Sci. USA* **108,** 3773–3778 (2011).
31. Warming, S., Costantino, N., Court, D. L., Jenkins, N. A. & Copeland, N. G. Simple and highly efficient BAC recombineering using galK selection. *Nucleic Acids Res.* **33,** e36–e36 (2005).
32. Datsenko, K. A. & Wanner, B. L. One-step inactivation of chromosomal genes in *Escherichia coli* K-12 using PCR products. *Proc. Natl Acad. Sci. USA* **97,** 6640–6645 (2000).
33. Yu, D. *et al.* An efficient recombination system for chromosome engineering in *Escherichia coli*. *Proc. Natl Acad. Sci. USA* **97,** 5978–5983 (2000).
34. Ficarro, S. B. *et al.* Improved electrospray ionization efficiency compensates for diminished chromatographic resolution and enables proteomics analysis of tyrosine signaling in embryonic stem cells. *Anal. Chem.* **81,** 3440–3447 (2009).
35. Askenazi, M., Parikh, J. R. & Marto, J. A. mzAPI a new strategy for efficiently sharing mass spectrometry data. *Nat. Methods* **6,** 240–241 (2009).
36. Ursell, T. S. *et al.* Rod-like bacterial shape is maintained by feedback between cell curvature and cytoskeletal localization. *Proc. Natl Acad. Sci. USA* **111,** E1025–1034 (2014).
37. Schindelin, J. *et al.* Fiji: an open-source platform for biological-image analysis. *Nat. Methods* **9,** 676–682 (2012).
38. Schneider, C. A., Rasband, W. S. & Eliceiri, K. W. NIH Image to ImageJ: 25 years of image analysis. *Nat. Methods* **9,** 671–675 (2012).
39. Gibson, D. G. *et al.* Enzymatic assembly of DNA molecules up to several hundred kilobases. *Nat. Methods* **6,** 343–345 (2009).
40. Jaqaman, K. *et al.* Robust single-particle tracking in live-cell time-lapse sequences. *Nat. Methods* **5,** 695–702 (2008).

Acknowledgements

The authors thank all members of the Bernhardt, Rudner and Garner laboratories for advice and discussions. The authors thank P. de Boer and C. Hale for the gift of the *mreB::galK* strain for constructing sandwich fusions and L. Lavis for his gift of JF dyes. This work was supported by the National Institutes of Health (R01AI083365 to T.G.B., AI099144 to T.G.B., CETR U19 AI109764 to T.G.B. and DP2AI117923 to E.C.G.). E.C.G. was also supported by a Smith Family Award and a Searle Scholar Fellowship. P.D.A.R. was supported in part by a pre-doctoral fellowship from CHIR. J.A.M. was supported by the Dana-Farber Strategic Research Initiative.

Author contributions

T.G.B., E.C.G., H.C., C.N.W., M.K., Z.B., P.D.A.R. and H.S. designed the experiments and wrote/edited the manuscript. H.C. performed the radiolabelling studies and constructed *E. coli* strains for physiological labelling and imaging studies. C.N.W. and M.K. performed imaging studies and analysis. Z.B. performed CDF analysis. H.C., H.S. and J.A.M. performed and analysed data from the liquid chromatography–mass spectrometry study of ^{MS}PBP1b modification. M.K. constructed *B. subtilis* strains. P.D.A.R. constructed and characterized the dominant-negative RodA variants and made *E. coli* PBP1a fusion strains for imaging.

Additional information

Supplementary information is available for this paper. Reprints and permissions information is available at www.nature.com/reprints. Correspondence and requests for materials should be addressed to E.C.G. and T.G.B.

Competing interests

The authors declare no competing financial interests.

© 2016 Macmillan Publishers Limited, part of Springer Nature. All rights reserved.